Effect of shape anisotropy in nanocrystals of semiconductors with small spin−orbit splitting *⊗*

S. V. Goupalov 🕶 📵

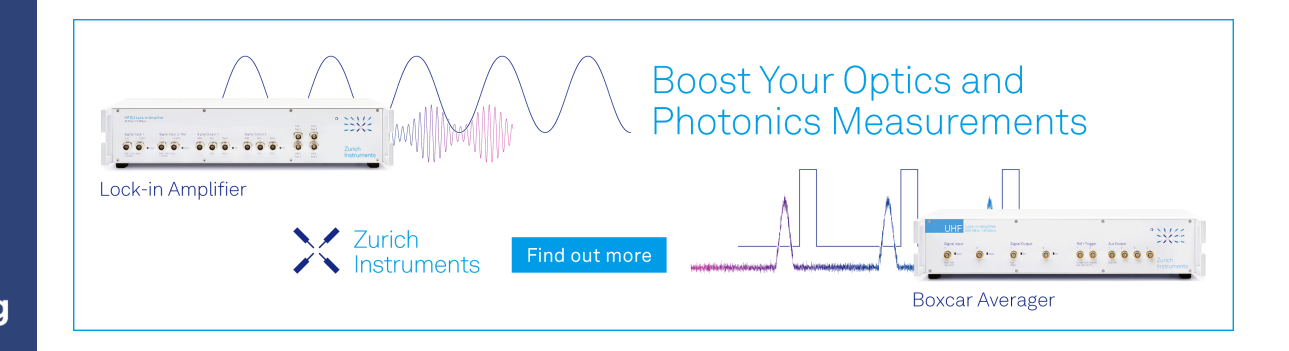


J. Chem. Phys. 160, 114703 (2024)

https://doi.org/10.1063/5.0187728









Effect of shape anisotropy in nanocrystals of semiconductors with small spin-orbit splitting

Cite as: J. Chem. Phys. 160, 114703 (2024); doi: 10.1063/5.0187728 Submitted: 15 November 2023 • Accepted: 3 March 2024 • Published Online: 20 March 2024







S. V. Goupalov^{a)}



AFFILIATIONS

Department of Physics, Jackson State University, Jackson, Mississippi 39217, USA and Ioffe Institute, 194021 St. Petersburg, Russia

^{a)}Author to whom correspondence should be addressed: serguei.goupalov@jsums.edu

ABSTRACT

We derive an effective spin-Hamiltonian accounting for the shape anisotropy of the zinc blende semiconductor nanocrystals within the k · p formalism explicitly taking into account the spin-orbit split-off valence band. It is shown that, for small InP nanocrystals, neglect of the spin-orbit split-off band can lead to significant underestimation of one of the two parameters determining the exciton fine-structure splittings. This parameter is only important for nanocrystals with shape anisotropy.

Published under an exclusive license by AIP Publishing. https://doi.org/10.1063/5.0187728

I. INTRODUCTION

Colloidal semiconductor nanocrystals are finding more and more applications. Their importance has been acknowledged with the 2023 Nobel Prize in Chemistry. Single quantum dot spectroscopy reveals that the symmetry of the nanocrystal shape, manifesting itself in the exciton fine structure splittings, is usually significantly lower than the symmetry of the underlying crystal lattice. 1,2 The simplest model accounting for the splittings is the model assuming that the nanocrystal has the shape of a triaxial ellipsoid.³ The observed small energy scale of the splittings allows one to consider such an ellipsoidal nanocrystal as a slightly deformed sphere. Since deformations are small, they are linear, which allows one to first consider a uniaxial deformation and then add up the results of the deformations along the three axes. 1-3 Uniform uniaxial deformations of the nanocrystal spherical shape were considered by Efros and Rodina in the model neglecting the spin-orbit split-off valence band.⁴ Recently, it has been shown⁵ that taking into account the admixture of the spin-orbit split-off band is crucial for calculating the effective g factor of top hole levels in CdSe and InP nanocrystals. The dark exciton states resulting from the fine-structure splitting can only be revealed in external magnetic fields mixing bright and dark zero-field states and leading to the brightening of the latter. Thus, a consistent description of the exciton fine structure in CdSe and InP nanocrystals within the $\mathbf{k} \cdot \mathbf{p}$ approximation should use the three-band model. The electron-hole exchange interaction, responsible for the exciton fine structure in quasi-spherical nanocrystals, has recently been considered within this model.⁶ In this paper, we elucidate the role of

the spin-orbit split-off band in the evaluation of the effect of the nanocrystal shape anisotropy.

II. HOLE STATES IN THE THREE-BAND MODEL

The isotropic three-band model describing the valence band structure of II-VI and III-V semiconductors utilizes the generalized Luttinger Hamiltonian, 9-11

$$\hat{H}(\mathbf{k}) = -\frac{\hbar^2 k^2}{2m_0} (\gamma_1 + 4\gamma) + \frac{3\hbar^2 \gamma}{m_0} (\mathbf{k}\hat{\mathbf{I}})^2 + \frac{\Delta}{3} (\hat{\boldsymbol{\sigma}}\hat{\mathbf{I}}) - \frac{\Delta}{3}, \tag{1}$$

where \hbar is Planck's constant, m_0 is the free electron mass, γ_1 and $y \equiv (2y_2 + 3y_3)/5$ are the Luttinger parameters, \hat{I}_{α} ($\alpha = x, y, z$) are the matrices of angular momenta I = 1, Δ is the spin-orbit splitting, and $\hat{\sigma}_{\alpha}$ are the Pauli matrices. The bands in a bulk semiconductor resulting from this Hamiltonian are shown in Fig. 1 for the case of zinc blende CdSe (the parameters are taken from Ref. 5). The most intuitive method of constructing states of a particle described by such a Hamiltonian and confined in a spherically symmetric potential was developed by Sercel and Vahala¹² for the two-band model and applied to the three-band model by Richard et al.8 It has also been demonstrated that the same method proves to be very efficient in describing the vibrational Lamb modes of spherical particles.¹³ The formalism is based on the fact that the differential operator $\hat{H}(-i\nabla)$ commutes with the operator of the total angular momentum $\hat{\mathbf{F}} = \hat{\mathbf{L}} + \hat{\mathbf{J}}$, where $\hat{\mathbf{L}} = -i\hbar \, \mathbf{r} \times \nabla$ and \hat{J}_{α} ($\alpha = x, y, z$) are the matrices of angular momenta, which can refer to both

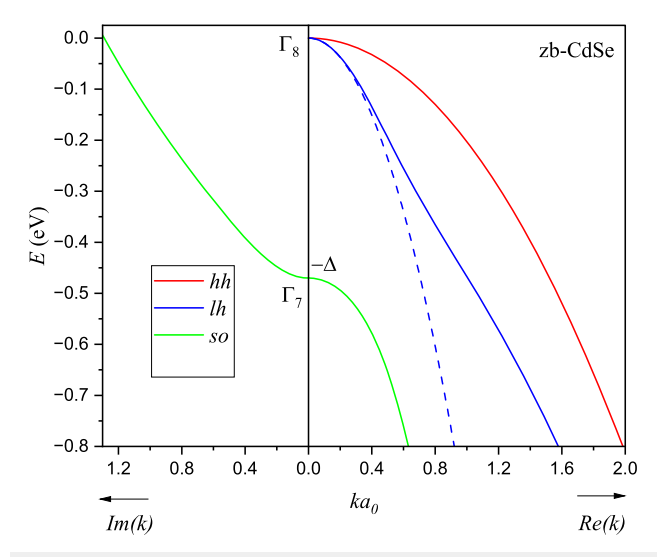


FIG. 1. In the two-band model, levels of size quantization of the valence-band hole originate from the parabolic bands of light (blue dashed line) and heavy (red solid line) holes. In the three-band model, the parabolic band of heavy holes is complemented by non-parabolic bands of the light (blue solid line) and spin-orbit split-off (green solid line) bands. The isotropic energy dispersion is shown in a vicinity of the Γ point of the Brillouin zone as a function of the dimensionless wave number ka_0 , where a_0 is the lattice constant. The Bloch functions at the Γ point transform under the Γ_8 (J=3/2) and Γ_7 (J=1/2) irreducible representations of the point group T_d . Within the two-band (three-band) model, to each energy correspond two (three) wave numbers from different bands.

J=3/2 and J=1/2. In what follows, however, we will only use the notation \hat{J}_{α} for J=3/2 and use the Pauli matrices for the case of J=1/2. The orbital angular momentum $\hat{\mathbf{L}}$ does not commute with $\hat{H}(-i\nabla)$. Thus, while the total angular momentum F serves as a good quantum number along with its projection F_z onto the z axis and the parity, several values of L, determined by the summation rules for angular momenta, usually contribute to each state of the confined hole. The lowest optically active exciton state is composed of the even hole state with total angular momentum F=3/2 and the ground electron state. The hole state is contributed by L=0, 2 for J=3/2 and by L=2 for J=1/2. Therefore, this state is labeled $1SDD_{3/2}$. In this paper, we will be concerned with only this hole state. It can be written as

$$|1SDD_{3/2}, F_z\rangle = \sum_{J,\nu} \mathcal{R}_{J,\nu;F_z}(\mathbf{r})|J,\nu\rangle,$$
 (2)

where $|J, v\rangle$ is the Bloch state at the top of the band Γ_8 when J = 3/2 or at the top of the band Γ_7 when J = 1/2 (cf. Fig. 1),

$$\mathcal{R}_{J,\nu;F_z}(\mathbf{r}) = \sum_{L} (-1)^{J-L+F_z} R_L^J(r)$$

$$\times 2 \sum_{M} \begin{pmatrix} J & L & \frac{3}{2} \\ \nu & M & -F_z \end{pmatrix} i^L Y_{LM} \left(\frac{\mathbf{r}}{r}\right), \tag{3}$$

where
$$\begin{pmatrix} J & L & \frac{3}{2} \\ v & M & -F_z \end{pmatrix}$$
 is the Wigner $3jm$ symbol that restricts possi-

ble values of L and M, $Y_{LM}(\frac{\mathbf{r}}{r})$ are the spherical harmonics satisfying $Y_{LM}^*(\frac{\mathbf{r}}{r}) = (-1)^M Y_{L-M}(\frac{\mathbf{r}}{r})$, and $R_L^J(r)$ are the hole radial wave functions satisfying zero boundary conditions at the nanocrystal surface and defined as follows:

$$R_{L}^{3/2}(r) = C \left[j_{L}(k_{hh}r) + \frac{(-1)^{L/2} k_{lh}^{2}(\rho_{so} + \chi_{so})}{k_{lh}^{2}(\rho_{so} + \chi_{so}) + k_{so}^{2}(\rho_{lh} - \chi_{lh})} \frac{j_{2}(k_{hh}a)}{j_{2}(k_{lh}a)} j_{L}(k_{lh}r) + \frac{(-1)^{L/2} k_{so}^{2}(\rho_{lh} - \chi_{lh})}{k_{lh}^{2}(\rho_{so} + \chi_{so}) + k_{so}^{2}(\rho_{lh} - \chi_{lh})} \frac{j_{2}(k_{hh}a)}{j_{2}(k_{so}a)} j_{L}(k_{so}r) \right],$$
(4)
$$R_{2}^{1/2}(r) = C \frac{m_{0}}{\gamma h^{2}} \frac{(\rho_{lh} - \chi_{lh}) (\rho_{so} + \chi_{so})}{k_{lh}^{2}(\rho_{so} + \chi_{so}) + k_{so}^{2}(\rho_{lh} - \chi_{lh})} \times j_{2}(k_{hh}a) \left[\frac{j_{2}(k_{lh}r)}{j_{2}(k_{lh}a)} - \frac{j_{2}(k_{so}r)}{j_{2}(k_{so}a)} \right].$$
(5)

Here, a is the nanocrystal radius, $j_L(x)$ is the spherical Bessel function of the order L, and we adapted notations of Ref. 8,

$$\rho(k) = \frac{1}{2m_0} \sqrt{9\gamma^2 \hbar^4 k^4 - 2\gamma m_0 \Delta \hbar^2 k^2 + m_0^2 \Delta^2}$$
$$\chi(k) = \frac{\Delta}{2} - \frac{\gamma \hbar^2 k^2}{2m_0},$$

 $\rho_{\eta} \equiv \rho(k_{\eta}), \ \chi_{\eta} \equiv \chi(k_{\eta}), \ \eta = lh, so.$ The wave number of the heavy holes is related to the hole energy through

$$k_{hh}^2 = \frac{2m_0|E|}{\hbar^2(\gamma_1 - 2\gamma)},$$

while those of the light and spin-orbit split-off holes satisfy the following equation:

$$\frac{\hbar^4 k^4}{4m_0^2} (\gamma_1 - 2\gamma)(\gamma_1 + 4\gamma) + \frac{\hbar^2 k^2 (\gamma_1 + 2\gamma)}{2m_0} \Delta - \frac{\hbar^2 k^2 (\gamma_1 + \gamma)}{m_0} |E| + |E|(|E| - \Delta) = 0.$$
(6)

One can see from Fig. 1 that, for E < 0, k_{lh}^2 is always positive, while, from Eq. (6),

$$k_{so}^2 = \frac{|E|(|E| - \Delta) \ 4m_0^2}{\hbar^4 k_{lb}^2 (\gamma_1 - 2\gamma)(\gamma_1 + 4\gamma)}$$

and becomes negative for $|E| < \Delta$, as shown in Fig. 1. In this case, one should make the following substitutions in Eqs. (4) and (5): $k_{so} \rightarrow i\kappa_{so}$, $j_L(k_{so}r) \rightarrow i^L i_L^{(1)}(\kappa_{so}r)$, and $j_L(k_{so}a) \rightarrow i^L i_L^{(1)}(\kappa_{so}a)$, where $i_L^{(1)}(x)$ is the modified spherical Bessel function.

The energy of the confined hole state is determined from the following dispersion equation:⁸

$$j_{0}(k_{hh}a)j_{2}(k_{lh}a)j_{2}(k_{so}a)\left[k_{lh}^{2}(\rho_{so}+\chi_{so})+k_{so}^{2}(\rho_{lh}-\chi_{lh})\right]$$

$$+j_{2}(k_{hh}a)\left[k_{lh}^{2}(\rho_{so}+\chi_{so})j_{0}(k_{lh}a)j_{2}(k_{so}a)\right]$$

$$+k_{so}^{2}(\rho_{lh}-\chi_{lh})j_{0}(k_{so}a)j_{2}(k_{lh}a)=0$$
(7)

for $|E| > \Delta$, and

$$j_{0}(k_{hh}a)j_{2}(k_{lh}a)i_{2}^{(1)}(\kappa_{so}a)\left[k_{lh}^{2}(\rho_{so}+\chi_{so})-\kappa_{so}^{2}(\rho_{lh}-\chi_{lh})\right]$$

$$+j_{2}(k_{hh}a)\left[k_{lh}^{2}(\rho_{so}+\chi_{so})j_{0}(k_{lh}a)i_{2}^{(1)}(\kappa_{so}a)\right]$$

$$+\kappa_{so}^{2}(\rho_{lh}-\chi_{lh})i_{0}^{(1)}(\kappa_{so}a)j_{2}(k_{lh}a)=0$$
(8)

for $|E| < \Delta$. The normalization constant $\mathcal C$ in Eqs. (4) and (5) is found from the condition,

$$\sum_{J,L} \int_{0}^{a} dr r^{2} [R_{L}^{J}(r)]^{2} = 1.$$

The results of the two-band model can be regained in the limit $\Delta \to \infty$. In particular, in this limit, $\rho_{so} + \chi_{so} \sim \Delta$, $\rho_{lh} - \chi_{lh} \sim 2\gamma^2 \hbar^4 k_{lh}^4 / \Delta m_0^2$. Therefore, Eq. (7) yields ^{7,12}

$$j_0(k_{hh}a)j_2(k_{lh}a) + j_2(k_{hh}a)j_0(k_{lh}a) = 0,$$

while from Eq. (4), we obtain

$$R_L^{3/2}(r) \to \mathcal{C} \left[j_L(k_{hh}r) + (-1)^{L/2} \frac{j_2(k_{hh}a)}{j_2(k_{lh}a)} j_L(k_{lh}r) \right].$$
 (9)

III. SHAPE ANISOTROPY

In order to account for the nanocrystal shape anisotropy, we will adapt an approach pioneered by Migdal^{14,15} who used it to find energy levels of a deformed nucleus. For nanocrystals, this approach was applied by Efros and Rodina within the two-band model.^{4,16} Consider a spheroidal nanocrystal with the surface,

$$\frac{x^2 + y^2}{b^2} + \frac{z^2}{c^2} = 1. {10}$$

Substituting $x \to bx/a$, $y \to by/a$, and $z \to cz/a$ transforms it into a sphere $x^2 + y^2 + z^2 = a^2$. Introducing the ellipsoidality parameter,

$$\mu_z = 2\frac{c-b}{c+b},\tag{11}$$

and assuming $|\mu_z| \ll 1$, from the condition $c b^2 = a^3$, one obtains

$$b \approx a \left(1 - \frac{\mu_z}{3}\right), \qquad c \approx a \left(1 + \frac{2\mu_z}{3}\right).$$

The above-mentioned change of variables also implies $k_{x,y} \rightarrow k_{x,y} (1 + \mu_z/3)$ and $k_z \rightarrow k_z (1 - 2\mu_z/3)$. When applied to the Hamiltonian (1), the latter receives the following addition:

$$\Delta \hat{H}(\mathbf{k}) = -\frac{\mu_z \hbar^2 (\gamma_1 + 4\gamma)}{m_0} \left(\frac{k^2}{3} - k_z^2 \right) + \frac{2\mu_z \hbar^2 \gamma}{m_0} (\mathbf{k}\hat{\mathbf{I}})^2$$
$$-\frac{3\mu_z \hbar^2 \gamma}{m_0} \left[(\mathbf{k}\hat{\mathbf{I}}) k_z \hat{I}_z + k_z \hat{I}_z (\mathbf{k}\hat{\mathbf{I}}) \right]. \tag{12}$$

Using explicit expressions for the Bloch wave functions, ^{10–12} one can write this Hamiltonian in the following basis,

$$|\mathbf{k}, J, \nu\rangle = \frac{e^{i\mathbf{k}\mathbf{r}}}{(2\pi)^{3/2}}|J, \nu\rangle.$$
 (13)

The Fourier transform of the matrix (3) can be formally considered as the following change of basis:

$$\langle \mathbf{k}, J, \nu | 1SDD_{3/2}, F_z \rangle = \frac{1}{(2\pi)^{3/2}} \int d\mathbf{r} e^{-i\mathbf{k}\mathbf{r}} \mathcal{R}_{J,\nu;F_z}(\mathbf{r})$$

$$\equiv \frac{1}{(2\pi)^{3/2}} \mathcal{R}_{J,\nu;F_z}(\mathbf{k}). \tag{14}$$

The anisotropy-induced correction to the hole energy can be calculated in the first order of the perturbation theory as matrix elements of the operator (12) on the functions (2). Inserting the unit operator expanded over the functions (13) and taking into account that matrix elements of the operator (12) on these functions are diagonal in ${\bf k}$, we obtain

$$\langle 1SDD_{3/2}, F'_{z} | \Delta \hat{H} | 1SDD_{3/2}, F_{z} \rangle = \frac{1}{(2\pi)^{3}} \sum_{J', \nu', J, \nu} \times \int d\mathbf{k} \ \mathcal{R}^{\dagger}_{F'_{z}, J', \nu'}(\mathbf{k}) \langle \mathbf{k}, J', \nu' | \Delta \hat{H}(\mathbf{k}) | \mathbf{k}, J, \nu \rangle \ \mathcal{R}_{J, \nu; F_{z}}(\mathbf{k})$$
(15)

or performing the angular integrations and summations,

$$\Delta \hat{H} = \frac{\mu_z \Delta_{sh}}{2} \left(\hat{J}_z^2 - \frac{5}{4} \right), \tag{16}$$

where

$$\Delta_{sh} = -\frac{\hbar^2}{6\pi^3 m_0} \int_0^\infty dk \, k^4 \left\{ \gamma \left(\left[I_0^{3/2}(k) \right]^2 - \frac{1}{5} \left[I_2^{3/2}(k) \right]^2 \right. \right. \\ \left. + \frac{7}{5} I_0^{3/2}(k) \, I_2^{1/2}(k) + \frac{1}{5} I_2^{3/2}(k) \, I_2^{1/2}(k) \right) \\ \left. + \frac{\gamma_1}{5} \left(2 \, I_0^{3/2}(k) \, I_2^{3/2}(k) + \left[I_2^{1/2}(k) \right]^2 \right) \right\}, \tag{17}$$

$$I_L^J(k) = 4\pi (-1)^{L/2} \int_0^a dr \, r^2 \, R_L^J(r) j_L(kr). \tag{18}$$

The form of Eq. (16) means that the shape anisotropy leads to splitting between the sublevels of the confined hole with $|F_z| = 3/2$

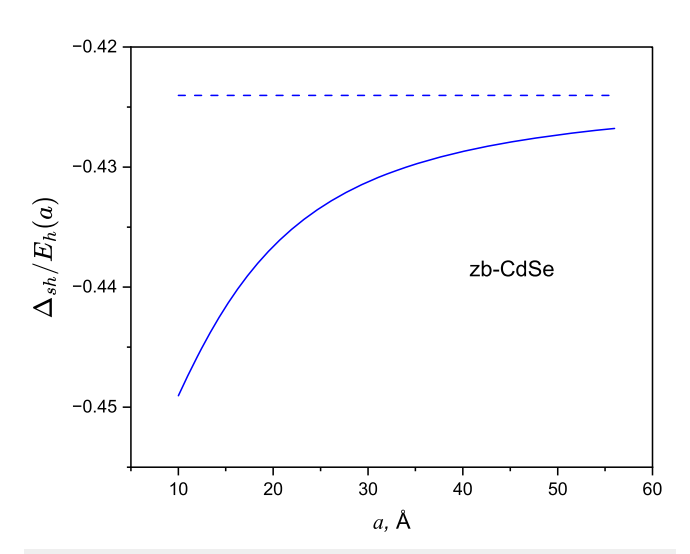


FIG. 2. Ratio of the characteristic energy Δ_{sh} to the unperturbed energy of the confined hole in the state $1SDD_{3|2}$ as a function of the zinc blende-CdSe nanocrystal radius calculated within the three-band (solid line) and two-band (dashed line) models. The two-band result corresponds to $2v(\beta)$ in terms of Ref. 4.

and $|F_z| = 1/2$. The splitting amounts to $|\mu_z \Delta_{sh}|$. To avoid confusion, we note that both the Hamiltonians (1) and (16) refer to the valence-band electron rather than the hole states (cf. Fig. 1).

When $\Delta \to \infty$, then $I_2^{1/2}(k) \to 0$, while $R_L^{3/2}(r)$ approach their two-band model limits according to Eq. (9). In this case, we obtain the two-band model result, which was given in Ref. 16 in a slightly different analytical form. In the two-band model, $R_L^{3/2}(r) = a^{-3/2} f_L(r/a)$, where $f_L(r/a)$ is the function depending on the ratio r/a. For this reason, as it follows from Eqs. (17) and (18), in the two-band model, $I_L^I(k) \propto a^{3/2}$ and $\Delta_{sh} \propto a^{-2} \propto E_h(a)$, where $E_h(a) > 0$ is the unperturbed energy of the confined hole in the

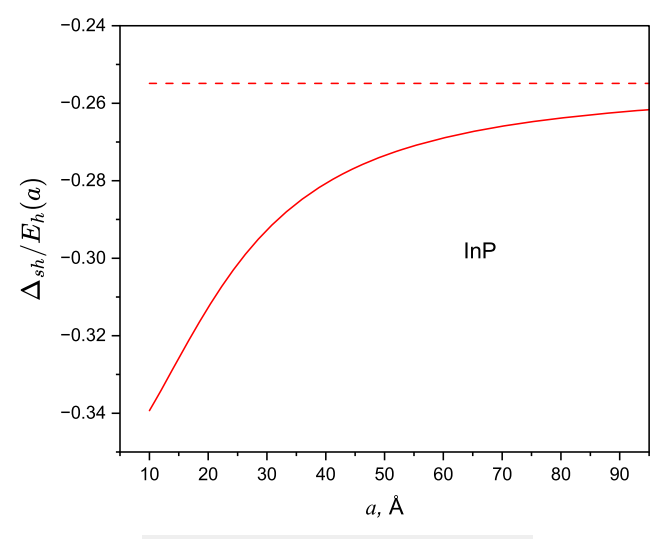


FIG. 3. Same as Fig. 2 but for InP nanocrystals.

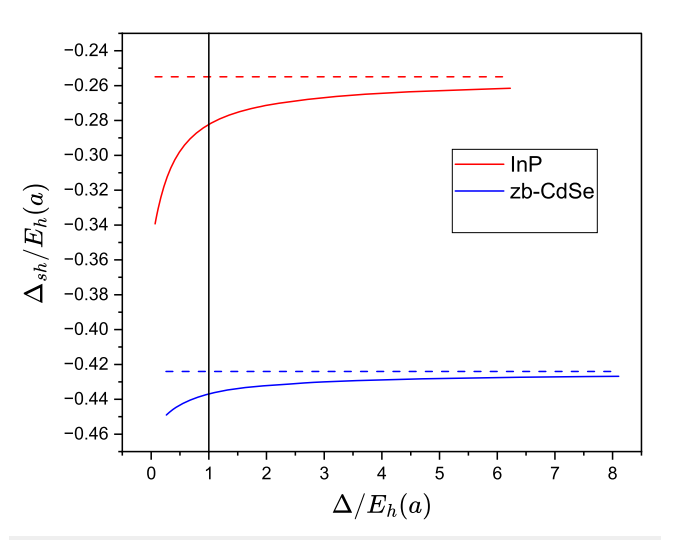


FIG. 4. Ratio of the characteristic energy Δ_{sh} to the unperturbed energy of the confined hole in the state $1SDD_{3/2}$ as a function of the ratio of the spin–orbit splitting to the same energy for InP (red lines) and zinc blende CdSe nanocrystals (blue lines). The dashed lines represent the corresponding two-band model limits $[2v(\beta)]$ in terms of Ref. 4].

ground state. In Figs. 2 and 3, we compare the results of the three-band and two-band models for the zinc blende CdSe and InP nanocrystals, respectively. We used the parameters in Refs. 5 and 8 for CdSe and InP nanocrystals, respectively. One can see that the ratio $\Delta_{sh}/E_h(a)$ in the three-band model becomes size-dependent. While for CdSe nanocrystals with relatively large spin–orbit splitting ($\Delta=470~{\rm meV}$), this dependence is not that strong, for InP nanocrystals ($\Delta=108~{\rm meV}$), the difference of the ratio from its two-band limit reaches 30% for small nanocrystals. Provided that the confinement energy scales as a^{-2} , the role of the shape anisotropy can be significantly underestimated by the two-band model for small InP nanocrystals.

Another illustration is shown in Fig. 4. Here, we plot the ratio of the characteristic energy Δ_{sh} to the unperturbed energy of the confined hole in the state $1SDD_{3/2}$ as a function of the ratio of the spin–orbit splitting to the same energy for InP and zinc blende CdSe nanocrystals. When $E_h(a) < \Delta$, the contribution of the spin–orbit split-off band to the hole wave function is associated with the purely imaginary wave number (cf. Fig. 1) and the ratio $\Delta_{sh}/E_h(a)$ asymptotically approaches the limit of $\Delta \to \infty$. When $E_h(a) > \Delta$, the spin–orbit split-off band contributes a real wave number and the difference from the two-band model becomes significant.

IV. EXCITON FINE STRUCTURE FOR A NANOCRYSTAL IN THE SHAPE OF A TRIAXIAL ELLIPSOID

Now, let us suppose that a spheroidal nanocrystal with the surface given by Eq. (10) is further stretched along the x direction and simultaneously squeezed along the y direction while preserving its elongation along the z axis. This yields a nanocrystal in the shape of a triaxial ellipsoid,

$$\frac{x^2}{b_x^2} + \frac{y^2}{b_y^2} + \frac{z^2}{c^2} = 1. {19}$$

One can introduce the in-plane anisotropy parameter

$$\mu_{xy} = 2 \frac{b_x - b_y}{b_x + b_y}$$

and assume that $|\mu_{xy}| \ll |\mu_z|$. This model³ allows one to describe the fine structure of the lowest optically active exciton state $1S_e1SDD_{3/2}$ in realistic colloidal quantum dots with zinc blende crystal lattice and strong carrier confinement.^{1,2} The resulting exciton fine structure is given by the following spin-Hamiltonian:^{1,3}

$$\hat{H}_X = -\eta_{exch}(\hat{\boldsymbol{\sigma}}\hat{\mathbf{J}}) - \frac{\mu_z \Delta_{sh}}{2} \left(\hat{J}_z^2 - \frac{5}{4}\right)$$

$$-\frac{\mu_{xy}\Delta_{sh}}{2}\left(\hat{J}_x^2-\hat{J}_y^2\right),\tag{20}$$

where η_{exch} is the electron-hole exchange energy, and we have neglected a small contribution due to the anisotropy of the long-range part of the electron-hole exchange interaction. The electron-hole exchange energy within the three-band model has recently been evaluated in Ref. 6, while the parameter Δ_{sh} is given by Eq. (17). The spin-Hamiltonian (20) leads to the splitting of the otherwise eightfold degenerate exciton level $1S_e1SDD_{3/2}$ into eight distinct sublevels^{1–3} even at zero external magnetic field. Analytic expressions for their energies may be found in Ref. 3.

V. CONCLUSIONS

We have studied how a uniform uniaxial deformation changing the spherical shape of a semiconductor nanocrystal to that of a prolate $(\mu_z>0)$ or oblate $(\mu_z<0)$ spheroid affects confined hole states. Ananalytical expression for the splitting of the confined hole state, contributing to the lowest optically active exciton, has been derived within the three-band model explicitly taking into account the spin–orbit split-off valence band. It is shown that, for small InP nanocrystals, neglect of the spin–orbit split-off band can lead to a significant underestimation of one of the two parameters determining the exciton fine-structure splitting. This parameter is only important for nanocrystals with shape anisotropy. Our results can be used to describe nanocrystals in the shape of triaxial ellipsoids, which provide an adequate model for realistic nanocrystal shapes. $^{1-3}$

ACKNOWLEDGMENTS

The author thanks Brahim Lounis and Philippe Tamarat for stimulating discussions. This work was supported by NSF through DMR-2100248.

AUTHOR DECLARATIONS

Conflict of Interest

The author has no conflicts to disclose.

Author Contributions

S. V. Goupalov: Writing – original draft (equal); Writing – review & editing (equal).

DATA AVAILABILITY

The data that support the findings of this study are available within the article.

REFERENCES

- ¹C. Sinito, M. J. Fernée, S. V. Goupalov, P. Mulvaney, P. Tamarat, and B. Lounis, "Tailoring the exciton fine structure of cadmium selenide nanocrystals with shape anisotropy and magnetic field," ACS Nano 8, 11651–11656 (2014).
- ²E. Prin, C. Xia, Y.-H. Won, E. Jang, S. V. Goupalov, P. Tamarat, and B. Lounis, "Revealing the band-edge exciton fine structure of single InP nanocrystals," Nano Lett. 23, 6067–6072 (2023).
- ³S. V. Goupalov, "Anisotropy-induced exchange splitting of exciton radiative doublet in CdSe nanocrystals," Phys. Rev. B **74**, 113305 (2006).
- ⁴ Al. L. Efros and A. V. Rodina, "Band-edge absorption and luminescence of nonspherical nanometer-size crystals," Phys. Rev. B 47, 10005 (1993).
- ⁵M. A. Semina, A. A. Golovatenko, and A. V. Rodina, "Influence of the spin-orbit split-off valence band on the hole g factor in semiconductor nanocrystals," Phys. Rev. B **104**, 205423 (2021).
- ⁶S. V. Goupalov, "Effect of finite spin-orbit splitting on the electron-hole exchange interaction in excitons confined in semiconductor nanocrystals," Phys. Rev. B **108**, 235419 (2023).
- ⁷ Al. L. Efros, "Luminescence polarization of CdSe microcrystals," Phys. Rev. B 46, 7448–7458 (1992).
- ⁸T. Richard, P. Lefebvre, H. Mathieu, and J. Allègre, "Effects of finite spin-orbit splitting on optical properties of spherical semiconductor quantum dots," Phys. Rev. B **53**, 7287–7298 (1996).
- ⁹M. I. Dyakonov and V. I. Perel, "Spin orientation of electrons associated with the interband absorption of light in semiconductors," Zh. Eksp. Teor. Fiz. **60**, 1954–1965 (1971) [Sov. Phys. JETP 33, 1053 1059 (1971)], see http://www.jetp.ras.ru/cgi-bin/dn/e_033_05_1053.pdf.
- ¹⁰ V. N. Abakumov, V. I. Perel, and I. N. Yassievich, Nonradiative Recombination in Semiconductors, Modern Problems in Condensed Matter Sciences, edited by V. M. Agranovich and A. A. Maradudin (Elsevier, New York, 1991), Vol. 33.
- ¹¹M. I. Dyakonov and V. I. Perel, "Theory of optical spin orientation of electrons and nuclei in semiconductors," in *Optical Orientation, Modern Problems in Condensed Matter Sciences*, edited by F. Meier and B. P. Zakharchenya (Elsevier, New York, 1984), Vol. 8.
- ¹²P. C. Sercel and K. J. Vahala, "Analytical formalism for determining quantum-wire and quantum-dot band structure in the multiband envelope-function approximation," Phys. Rev. B **42**, 3690–3710 (1990).
- $^{1\hat{3}}$ S. V. Goupalov, "Classical problems in the theory of elasticity and the quantum theory of angular momentum," Usp. Fiz. Nauk **190**, 63–72 (2020), [Physics-Uspekhi 63, 57–65 (2020)].
- ¹⁴A. B. Migdal, Qualitative Methods in Quantum Theory (W.A. Benjamin, Reading MA, 1977).
- ¹⁵L. D. Landau and E. M. Lifshitz, Quantum Mechanics. Non-relativistic Theory, 3rd ed. (Pergamon Press, Oxford, 1977).
- ¹⁶A. V. Rodina and A. L. Efros, "Band-edge biexciton in nanocrystals of semiconductors with a degenerate valence band," Phys. Rev. B 82, 125324 (2010).